DOI: 10.2478/ata-2025-0023

Acta Technologica Agriculturae 3
Nitra, Slovaca Universitas Agriculturae Nitriae, 2025, pp. 183–190

ACOUSTIC EMISSION CONTROL OF COMPOUNDS WITH INTERFERENCE, WHICH ARE ASSEMBLED BY THERMAL METHOD

Mykola ZENKIN[1], Serhii LISOVETS[2], Dmytro MAKATORA*[1], Ján KOSIBA[3]

[1]National Technical University of Ukraine, Igor Sikorsky Kyiv Polytechnic Institute, Educational and Scientific Institute for Publishing and Printing, Department of Printing Machines and Automated Complexes, Kyiv, Ukraine, nikolay_zenkin@ukr.net
[2]V. I. Vernadsky Taurida National University, Educational and Scientific Institute of Municipal Administration and Urban Economy, Department of Engineering Systems and Technologies, Kyiv, Ukraine, ser.lis.290171@gmail.com
[3]Slovak university of Agriculture in Nitra, Faculty of Engineering, Institute of Agricultural Engineering, Transport and Bioenergetics, Nitra, Slovakia, jan.kosiba@uniag.sk

*correspondence: makatora_d@ukr.net

Acoustic emission control means for tension connections are proposed. The features of the contact zone, such as the gas gap between the shaft and the bushing and the penetration of microroughnesses of the shaft surface into the bushing surface, are considered. It is shown that the main indicator of such compounds is total acoustic emission. It has been established that with increasing tension, the maximum intensity of acoustic emission signals is observed earlier, and their amplitude becomes larger. In addition, it has been found that total acoustic emission depends on the strength of joints and the magnitude of total acoustic emission can determine this strength. The paper presents the results of studies of several series of experimental and field samples. It has been established that the greater the intensity of acoustic emission signals and the lower the total acoustic emission, the stronger the tension bonds. It has been established that there is no direct relationship between the intensity of acoustic emission signals and the contact surface area, but with an increase in the contact area, total acoustic emission also increases.

Keywords: contact zone; connection; sample; tension; contact surface area; landing diameter; compression

Due to their reliability, simplicity, and manufacturability, tension joints assembled by thermal method are widely used in various machines and mechanisms. Health and safety in the workplace are an important part of the management systems of organisations and government bodies in most countries of the world (Žitňák et al., 2023). One of their varieties is cylindrical joints (Liu et al., 2024), which are assembled by cooling the shaft to a low temperature (detail/part which is covered) at a room temperature of the bushing (detail/part which covers). With proper quality control, such joints can be strong and long-lasting. The process of their assembly is well automated (Ohtsu, 2015; Bagheri et al., 2024).

The studies of tension joints assembled by thermal method show that the main inhibiting factor of their manufacturing technology is the lack of reliability of existing control methods (Zhang et al., 2019a). Of the existing control methods, the most promising is acoustic emission (AE). Nowadays, condition monitoring (CM) along with early and continuous fault diagnosis (FD) (Alshorman et al., 2021) are vital in the modern life of industries (Rani et al., 2020). The importance of CM and FD engineering processes comes from a serious need for continuous monitoring of the health of industrial components (Zhang et al., 2019b) and systems through their life (Zhao et al., 2020). When assembling joints under the influence of normal and tangential forces, dislocation movement occurs in the contact zone between the shaft and the bushing, which is the source of AE. Several processes take place in this zone, the main of which is the deformation process caused by friction between the surfaces of the shaft and the bushing when connected (Lacagnina et al., 2021).

Depending on the value of tension (radial pressure), deformations on the contact surface can be both elastic and elastic-plastic. The most typical case of contact zone formation in tensioned joints is when the shaft is assembled into the hole exclusively through cooling.

The cooling of the shaft to low temperatures at a bushing temperature close to the ambient temperature leads to a decrease in the diameter of the shaft and the formation of a technological gap (air layer) (Nashed et al., 2013). After the shaft is reheated, the microroughness of the surfaces of the shaft and the bushing comes into contact (Bertagnolio et al., 2017). Once the temperatures of the shaft and the bushing are equalised, the technological gap reaches its minimum value (Jiang et al., 2014).

The influence of contact pressure, contact heat transfer, and the nature of contacting micro-irregularities on total AE was determined. In addition, the dependence between the increase in tension and the moment when AE signals reach the maximum intensity was established. Moreover, a correlation was also established between the increase in tension and the amplitude of AE signals. Another achievement of the study was to determine the effect on the AE of both temperature equalisation in the contact zone of the shaft and the bushing and the formation of the contact zone. The results of the study make it possible to obtain a "passport" of the contact connection, having information about total AE and the contact surface area.

Material and methods

The research method involved the selection of samples of the bushing and shaft, which will form a connection with tension, as well as equipment designed to establish the relationship between the strength of such a connection and the distribution of pulses of AE during its assembly.

The peculiarity of the contact zone of joints with tension is that, in addition to the areas of direct contact of the shaft with the bushing, there is also a gas layer between them, in which there is almost no convection. Therefore, the equalisation of the temperatures of the shaft and the bushing can be carried out both through the areas of direct contact and through this gas layer. Another feature of deep cold assembly is the predominant penetration of microroughness of the shaft surface (detail/part which is covered) into the surface of the bushing (detail/part which covers). In this case, both the surface of the bushing and microroughness on it change significantly. This effect is most clearly manifested at the shaft temperature from -80 °C and below. At the same time, in the surface of the shaft, there are elastic deformations, and in the surface of the bushing – elastic-plastic deformations. The analysis of the processes that take place in the contact area shows that at the time of the initial contact of the surfaces of the bushing and the shaft, the surface of the bushing "sticks" to the surface of the shaft, and this state is maintained until complete connection.

At each contact of microroughnesses of the surfaces of the shaft and the bushing, the pulses of AE are generated. The set of these pulses forms total AE. The process of increasing the areas of direct contact of the shaft with the bushing and, accordingly, the increase of total AE continues until there is a temperature difference between the surfaces of the shaft and the bushing and while radial pressure increases. Total AE is interrelated with the actual contact area of the shaft and bushing surfaces and can be used as an informative parameter to control the strength of the connection between the shaft and the bushing.

It can be assumed that one elementary movement of one section of direct contact of the shaft with the bushing generates one pulse AE – that is, such a pulse that can be recorded with high probability. In turn, knowing the total number of areas of direct contact of the shaft with the bushing and the total movement of each of these areas, one can determine the total AE. The total movement of the areas of direct contact of the shaft with the bushing is significantly affected by factors such as contact time and temperature difference between the surfaces of the shaft and the bushing.

Pulse AE during generation is propagated through the material of the shaft and the bushing and ultimately received by the sensor of AE. The spectrum of such a momentum can be represented, according to Fourier transform, as an infinite set of harmonic oscillations. When the AE pulse propagates through the material, such phenomena as the dispersion of acoustic waves with different frequencies, the transformation of types of acoustic waves, numerous reflections of acoustic waves, etc. occur. When detecting AE pulses using sensors based mainly on piezoelectric ceramics, several additional phenomena may occur. These include uneven amplitude-frequency characteristics of the sensor, reflections of acoustic waves from the back of the plate and the sensor housing, the presence of resonant peaks, and nonlinearities of the piezoelectric ceramic material. Thus, the pulse shape of AE, which is generated at one site of direct contact of the shaft with the bushing, and the pulse shape of AE, which is obtained at the output of the signal amplifier of AE, can differ significantly.

In Fig. 1, it is possible to observe both the natural resonant frequencies of the tension connection and the natural resonant frequencies of the sensor (piezoelectric ceramics). A typical form of experimentally obtained pulse AE is shown in Fig. 2. The duration of such pulses is approximately 1 ms, and filling frequency is in the range from 50–200 kHz to 1.0–1.2 MHz.

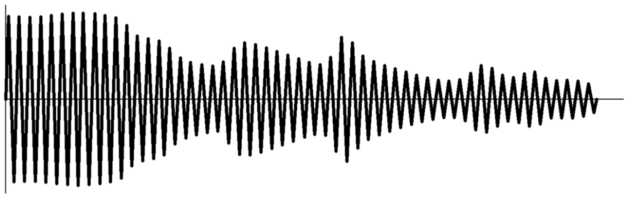

Fig. 1 A typical form of experimentally obtained pulse AE
Source: Narayanan et al., 2024; Kovacevic et al., 2002

As can be seen in Fig. 1, pulse AE has a complex shape, and from pulse to pulse, this shape will vary significantly. To calculate the total AE, it is desirable that one pulse of AE emits one information pulse (for example, rectangular). Thus, counting the total number of such information pulses, one can determine the total AE. This is usually achieved by introducing a set level of discrimination and a "time window" for AE pulse (for example, as shown in Fig. 2).

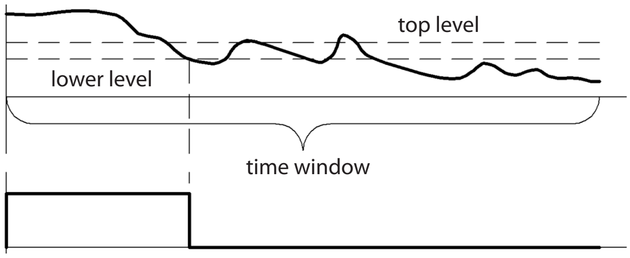

Fig. 2 Introduction of a given level of discrimination for the envelope pulse AE

Therefore, total AE can be determined by the following simple formula:

$$AE_{\Sigma} = \sum_{i=1}^{N} n_i \tag{1}$$

where: AE_{Σ} – total AE; – the number of areas of direct contact of the shaft with the bushing; n_i – the number of elementary movements of the i^{th} section

Thus, having information about total AE, it is possible to predict the operational reliability of tension connections collected by thermal method. The purpose of the research is to provide an opportunity to develop the "passports" of tension connections. Having obtained once for a certain connection with tension the distribution of pulses of AE during its assembly, on the basis of this distribution, it will be possible to predict the operational reliability of similar connections.

To achieve this goal, one needs to solve the following tasks. Firstly, it is a justification of the factors that affect the total AE and determine the nature of this effect. Secondly, it is an experimental confirmation of obtained theoretical dependences. According to research results, total AE depends on such basic factors as contact pressure, contact heat transfer, and the nature of contact of microroughnesses.

The most easily measurable contact heat transfer (Fig. 4 as an example) shows the parameters of such heat transfer between the shaft and the bushing, which have the same length of 60 mm. The diameter of the bore is 50 mm, and the outer diameter of the bushing is 100 mm. The measurement was performed at two tensions: 30 µm and 70 µm. In Fig. 4, the change in the temperature of the middle part of the shaft is indicated by position 1, the outer surface of the shaft is position 2, the inner surface of the bushing is position 3, and the outer surface of the bushing is position 4.

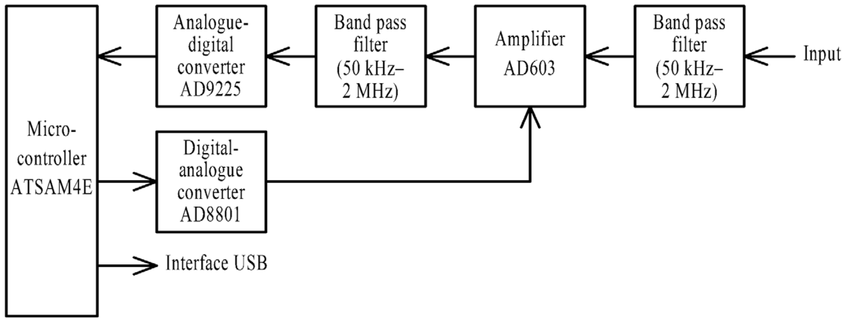

Fig. 4 Simplified block diagram of the module registration of AE signal shape

The graphs in Fig. 3a and Fig. 3b are almost the same, except that the heat exchange under tension 70 µm proceeds approximately 1.5 faster than the heat exchange under tension 30 µm. The analysis of these tension connections showed that as tension increases from 30 µm to 70 µm, the contact surfaces of the shaft and the bushing converge by about 10–20% and the number of contact areas increases slightly by more than twice. In this case, in the contact zone, along with elastic deformation, plastic deformation associated with the rooting of microroughnesses of the shaft surface in the surface of the bushing increases sharply. This leads to a significant increase in the contact area and a decrease in the total movement of the contact areas. In addition, the number of pulses of AE decreases from 11275 to 3874, and allowable load on the connection increases from 159 kN to 470 kN.

An original measuring transducer based on piezoceramics made of lead zirconate-titanate was used for research. As part of the equipment, a signal processing module for AE was used. It was developed based on the results of previous research on AE detection methods (Pomponi et al., 2015; Agletdinov et al., 2016), acoustoelectric converters (Beranek and Mellow, 2019), noise reduction techniques (Danyuk et al., 2014; Pomponi and Vinogradov, 2013), high-reliability converters (Danyuk et al., 2017), and signal filtration systems (Barat et al., 2016). The main purpose of the module was to register the form of AE signals with their subsequent transfer via USB to a personal computer, which carried out all the further processing of these signals (Builo, 2013). It was found that the direct transmission of information about AE signals to a personal computer without its pre-processing did not allow to process AE signals at a speed greater than approximately 100 imp·sec^{-1}. The growth of the same pre-processing of AE signals allowed an easy increase to values 1000 imp·sec^{-1}. A simplified block diagram of the AE signal shape registration module is shown in Fig. 4.

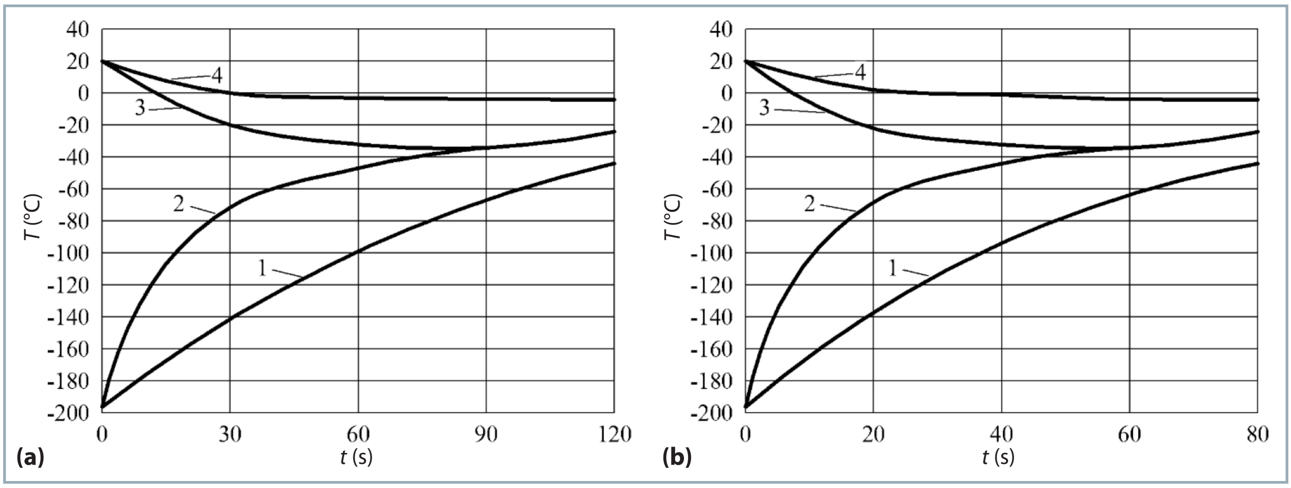

Fig. 3 Change of temperatures of the shaft and the bushing
(a) – tension 30 µm; (b) – tension 70 µm

Acoustic emission signals from the transducer came through the first bandpass filter with a bandwidth of 50 kHz – 2 MHz and were amplified by an amplifier with adjustable gain AD603. Such an amplifier could either directly amplify the signal or attenuate it depending on what control voltage was supplied to it from the digital-to-analogue converter AD8801. After that, amplified signal passed through the second bandpass filter with the same bandwidth of 50 kHz – 2 MHz and was digitised by a high-speed parallel analogue-to-digital converter AD9225.

Data processing from AD9225 and the operation control of AD8801 was performed using a microcontroller with ARM-architecture ATSAM4E, which operated at frequency 120 MHz. In contrast to the board (Beranek and Mellow, 2019) that allowed the calculation of various parameters of AE signals (amplitude, duration, energy, etc.), the purpose of the developed module was the most reliable determination of the presence or absence of AE pulses. Data exchange with the personal computer was carried out via the USB interface at speed 12 Mbit·sec^{-1} (Breckenridge et al., 2005; Carlos et al., 2005).

Results and discussion

The studies were performed on both experimental and field samples, which were used in two and three series, respectively. The first series of experimental samples had a bore diameter of 50 mm and a length of 60 mm; for the second series, these values were 25 mm and 30 mm, respectively (Fig. 5). Both the first and second series of experimental specimens were divided into three groups of 10 specimens in each group, and their assembly was carried out according to the minimum, average, and maximum strains with H7/r6 bore. For the first series, the minimum tension was in the range of 0.029–0.031 mm, average tension – 0.048–0.053 mm, the maximum tension – 0.067–0.073 mm; for the second series, these values were 0.005–0.010 mm, 0.021–0.027 mm, and 0.035–0.043 mm, respectively.

The first series of field samples was a connection "car axle PU1 – solid roller wheel", the second series had a landing diameter of 30 mm and a length of 30 mm (Fig. 6), and for the third series, these values were 52 mm and 60 mm, respectively (Fig. 7). The second and third series of field samples were the connection "shaft – gear", which is used in motor reducers MC2C-100H and reducers C2U-315H.

For the first series, the minimum tension was 0.120 mm, average tension 0.140 mm, and the maximum

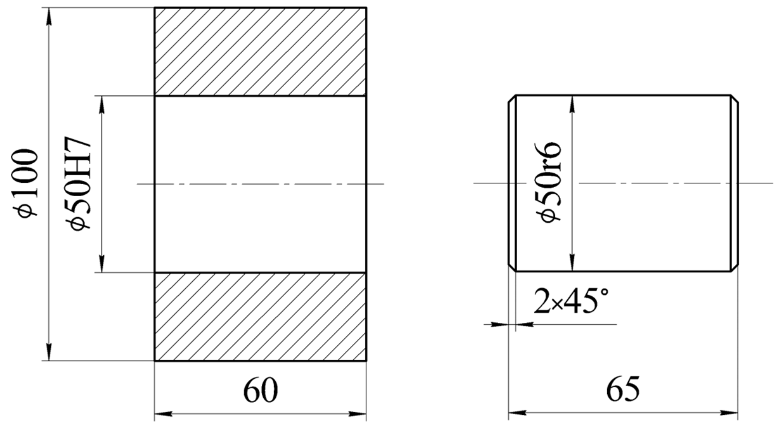

Fig. 5 Experimental sample of the bushing and shaft (bore diameter 50 mm)

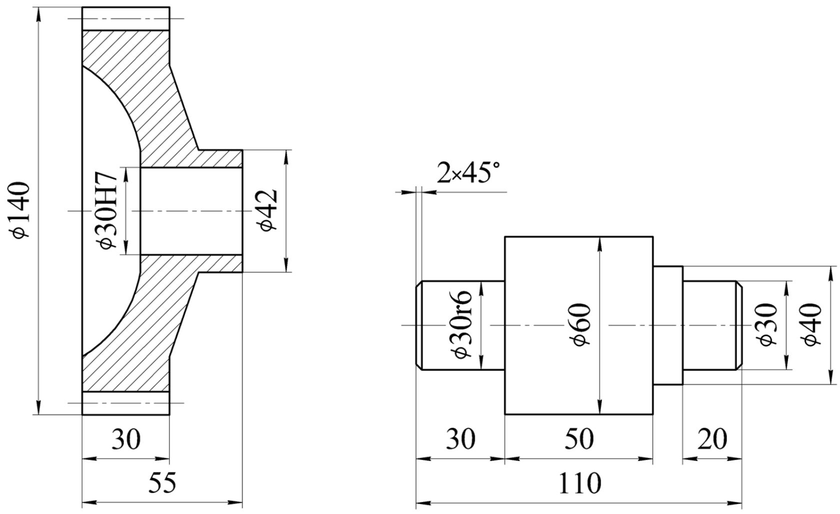

Fig. 6 Full-scale sample of the bushing and shaft (bore diameter 30 mm)

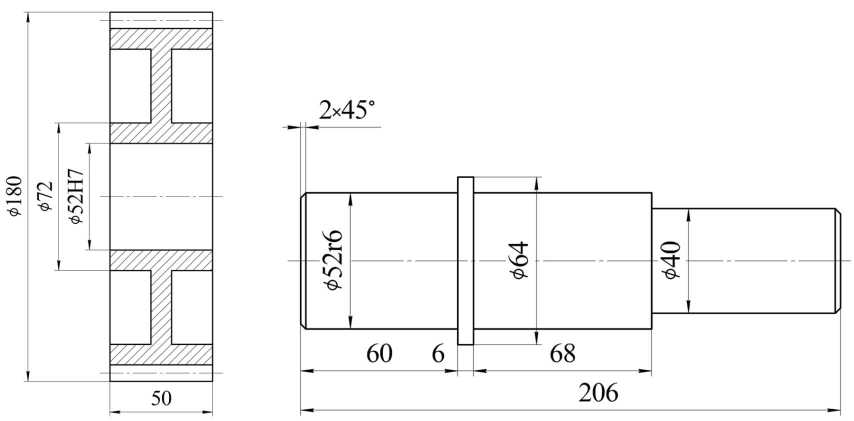

Fig. 7 Full-scale sample of the bushing and shaft (bore diameter 52 mm)

tension 0.160 mm; for the second series, these values were 0.031 mm, 0.038 mm, and 0.043 mm, respectively; and for the third series 0.034 mm, 0.049 mm, and 0.057 mm, respectively. The control of AE signals was performed directly during the formation of the interference fit when the shaft, cooled to approximately -196 °C, was inserted into the hole of the bushing. After that, the bushing was heated to achieve the required tension. The processing of research results allowed us to receive dependences between tension and total AE.

Figure 8 shows the dependences of the intensity of AE signals on time, obtained through every 10-sec experimental samples of the first series with the minimum (30 μm), average (50 μm), and maximum (70 μm) tensions. The analysis of these dependences shows that with increasing tension, the maximum intensity of AE signals is observed earlier, and its amplitude becomes larger. The formation time of the contact zone of joints with the maximum tension (70 μm) is about three times, and the formation time of the contact zone of joints with average tension (50 μm) is about twice less than the formation time of the contact zone of joints with the minimum tension (30 μm).

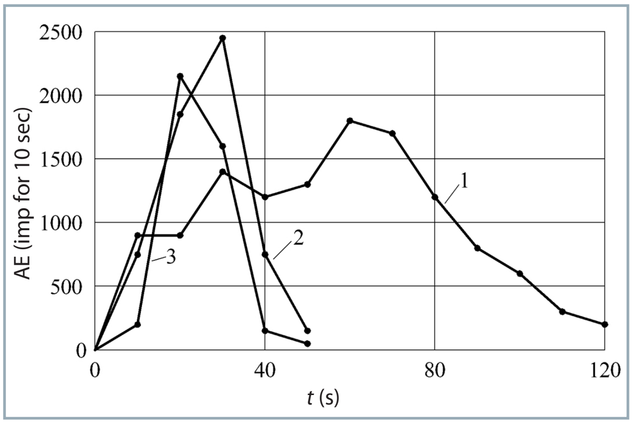

Fig. 8 The signal intensity of the AE experimental samples of the first series
1 – tension 30 μm; 2 – tension 50 μm; 3 – tension 70 μm

It was found that the maximum AE signal intensity of experimental samples with tension 30 μm was achieved in the time interval from 53 sec to 70 sec, with tension 50 μm – from 23 sec to 38 sec, and with tension 70 μm – from 15 sec to 23 sec. The duration of the maximum intensity of AE signals for different voltages was 17 sec, 15 sec, and 8 sec, respectively. The dependences of total AE on time for such experimental samples are shown in Fig. 9. For the above tensions, total AE averaged 12,000, 6000, and 4000 imp, respectively. It was also found that after equalisation of temperatures in the contact zone of the shaft and the bushing the formation of the contact zone AE completely stops.

Thus, it can be argued that with increasing tension, the intensity of AE signals increases, but total AE decreases. After measuring the AE signals of the experimental samples, the joints were depressed, and the connections were pressed. At the same time, it was found that average depressing force is 150 kN for tension 30 μm and 444 kN for tension 70 μm. The strength of interference joints

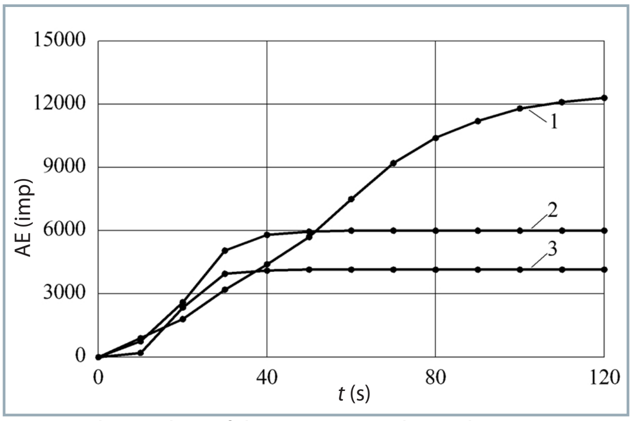

Fig. 9 The total AE of the experimental samples of the first series: 1 – tension 30 μm; 2 – tension 50 μm; 3 – tension 70 μm

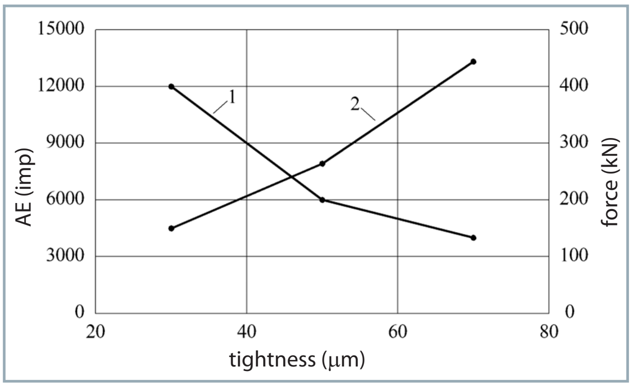

Fig. 10 Effect of tension on connection parameters
1 – dependence "tension – total AE"; 2 – dependence "tension – strength of connections with tension"

assembled using the thermal method depends directly on the tension applied. It has been observed that total AE correlates with joint strength, which makes it possible to estimate this strength based on the total AE value. Thus, the research results of experimental samples in principle allow connecting the total AE (on one hand) and the strength of tension joints assembled by thermal method (on the other hand). This dependence is shown in Fig. 10.

Therefore, the process of assembling tension joints thermally can be divided into three stages. In the first stage, individual bursts of AE signals are registered, which corresponds to the beginning of the process of convergence of contact surfaces and their mutual rooting. This radiation does not characterise the strength of the connection.

In the second stage, the maximum intensity of AE signals is observed, which corresponds to the process of active convergence of a large number of microroughnesses of the shaft and bushing surfaces, the presence of plastic deformations during their mutual rooting, and the crumpling of microroughnesses in deeper layers of the contact zone. It is this radiation that characterises the strength of the connection.

In the third stage, the intensity of AE signals decreases significantly. This stage corresponds to the completion of plastic deformation of microroughnesses of the shaft and bushing surfaces. This radiation also does not characterise the strength of the connection. The stronger the tension

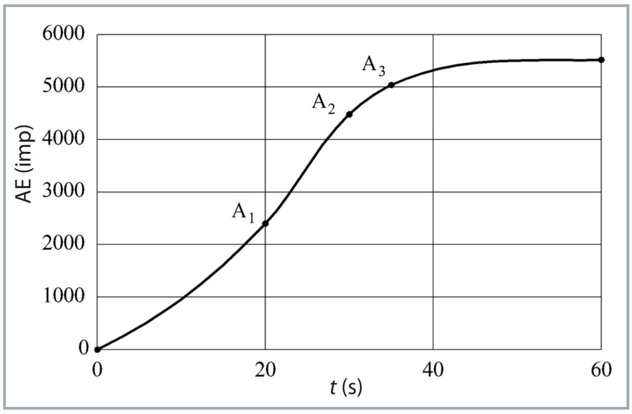

Fig. 11 Total AE connection "shaft – gear"

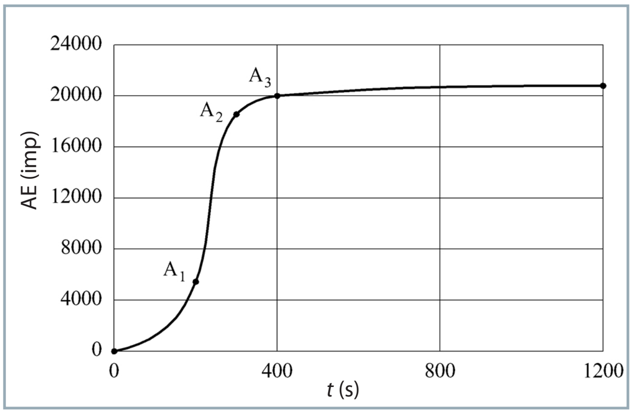

Fig. 12 Total AE connection "car axle PU1 – solid rolled wheel"

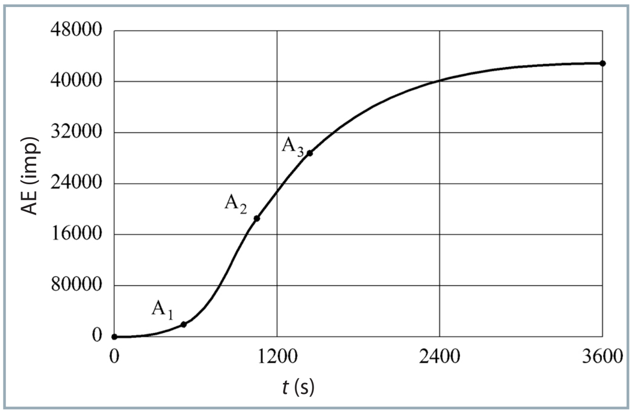

Fig. 13 Total AE connection "wheel – bandage"

connections, the greater the intensity of AE signals and the smaller the total AE. For the second series of experimental samples, as well as for the first, second, and third series of field samples, the dependences "tension – total AE" and "tension – strength of connections with tension" were obtained, which were similar to the dependences obtained for the first series of experimental samples (Fig. 11).

Three series of connections were used to study the effect of geometric dimensions of tension joints on the strength of AE signal and total AE. There were 5 samples in each series. The first series of connections had a landing diameter of 52 mm (connection "shaft – gear wheel" in reducers C2U-315H), the second – 196 mm (connection "car axle PU1 – solid rolled wheel"), the third – 900 mm (connection "wheel – bandage"). During the research, it was found that with increasing contact surface, the formation time of the contact zone, total AE, and compressive force increased, and the intensity of AE signals per unit contact surface decreased.

The dependences of total AE on time for the first series of connections are shown in Fig. 11, for the second series of connections – in Fig. 12, and for the third series of connections – in Fig. 13.

As can be seen, in the areas of the curves from the beginning of measurement to point A_1, the intensity of AE signals gradually increases. In the areas from point A_1 to point A_2, the intensity of AE signals reaches its maximum value; these areas serve as a criterion for determining the strength of tension joints assembled by thermal method. In the areas from point A_2 to point A_3, the intensity of AE signals gradually decreases. In the areas after point A_4 and until the end of measurement, the intensity of AE signals decreases to almost zero.

The dependence of AE signals intensity on the contact surface area is shown in Fig. 14. As shown in Fig. 14, the intensity of AE signals in joints under tension initially decreases with an increase in the contact surface area – from 0.66 to 0.17 imp·sec^{-1} – and then rises sharply to 1.78 imp·sec^{-1}. However, since there can be a complex ambiguity between the intensity of AE signals and the surface area of the contact, it is not possible to estimate the strength of tensile joints by the value of the intensity of AE signals.

The dependence of total AE on the contact surface area is shown in Fig. 15. As can be seen from Fig. 15, the total AE of tension joints increases with contact surface area: first gradually, from 5960 to 21,250 impulses, and then rapidly to 433,629 impulses. Since total AE increases monotonically with the growth of the contact surface area, it is recommended to use the total AE value as a parameter for evaluating the strength of tension joints.

Therefore, the tension strength of connection can be determined by having information about total AE and contact surface area, thus creating a "passport" of such a connection.

The "passport" of connection can be presented in the form of tables, graphs, formulas, or in several different ways at the same time.

The descriptions of acoustic-based fault diagnosis techniques are also available in the literature (O´Brien et al., 2017; Wang et al., 2016). The advantages of acoustic-based

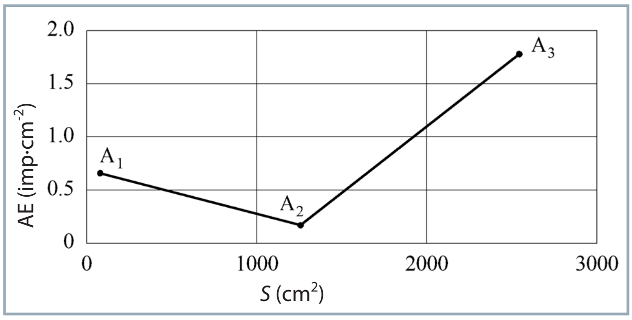

Fig. 14 The intensity of AE signals depending on the contact surface area

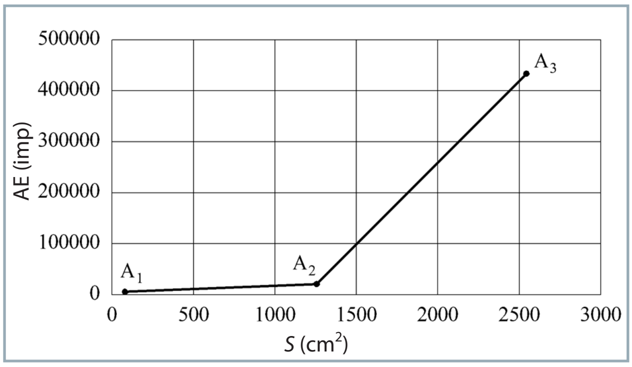

Fig. 15 Total AE depending on the contact surface area

fault diagnosis are: non-invasive technique, low cost, and instant measurement of acoustic signals (Glowacz, 2018). More importantly, some researches illustrated that feature representation extracted by a good deep neural network has one measuring standard (Zhao et al., 2020; Xu et al., 2017). Chan and Stolfo (1998) introduce an approach to explore majority class examples, they split the majority class into several non-overlapping subsets, and finally ensemble classifiers using stacking (Wu et al., 2018). Namely, the perturbation of inputting data to a certain extent does not deform, which can avoid the phenomenon of over-fitting (Shao et al., 2018).

Conclusion

The proposed method and technical solution for the AE control of tension joints assembled using the thermal method enables, with relative simplicity, the reliable determination of joint strength, particularly compressive strength. The results highlight the importance of accounting for the gas layer that may form between the shaft and the bushing during assembly. It is established that the main source of AE signals is the penetration of shaft's surface microroughnesses into the bushing surface upon contact.

To register the waveform of AE, the equipment based on an ARM-based microcontroller (ATSAM4E) was developed, incorporating the features of existing designs. The study also demonstrates that total AE is the most informative parameter for assessing the strength of thermally assembled tension joints. Therefore, it is essential to consider the contact surface area between the shaft and the bushing, which can be experimentally measured or theoretically calculated. Given the total AE value for a specific joint type and assembly conditions, it is possible to generate a "passport" for such connections.

When performing AE control, measuring the total AE makes it possible to generate a "passport" for the joint, which can be used to determine the compressive force of tension joints. The studies conducted on multiple series of experimental and field samples have confirmed the effectiveness and efficiency of this method for the quality assessment of tension joints.

Acknowledgment

We would like to express our sincere gratitude to the administration of the Department of Printing Machines and Automated Complexes of the National Technical University of Ukraine "Igor Sikorsky Kyiv Polytechnic Institute" for their support and cooperation.

References

AGLETDINOV, E. – POMPONI, E. – MERSON, D. – VINOGRADOV, A. 2016. A novel Bayesian approach to acoustic emission data analysis. In Ultrasonics, no. 72, pp. 89–94. DOI: https://doi.org/10.1016/j.ultras.2016.07.014

ALSHORMAN, O. – ALKAHATNI, F. – MASADEH, M. – IRFAN, M. – GLOWACZ, A. – ALHOBIANI, F. – KOZIK, J. – GLOWACZ, W. 2021. Sounds and acoustic emission-based early fault diagnosis of induction motor: A review study. In Advances in Mechanical Engineering, vol. 13, no. 2. DOI: https://doi.org/10.1177/1687814021996915

BAGHERI, A. – TARIGHI, J. – EMAMI, N. – SZYMANEK, M. 2024. Extension experts´ intentions to use precision agricultural technologies, a test with the technology acceptance model. In Acta Technologica Agriculturae, vol. 27, no. 2, pp. 84–91. DOI: https://doi.org/10.2478/ata-2024-0012

BARAT, V. A. – CHERNOV, D. V. – ELIZAROV, S. V. 2016. Discovering data flow discords for enhancing noise immunity of acoustic-emission testing. In Russian Journal of Nondestructive Testing, vol. 52, no. 6, pp. 347–356. DOI: https://doi.org/10.1134/S1061830916060024

BERANEK, L. – MELLOW, T. 2019. Acoustics: Sound Fields, Transducers and Vibration. UK : Elsevier, Academic Press, 900 pp. ISBN 978-0-12-815227-0. DOI: https://doi.org/10.1016/C2017-0-01630-0

BERTAGNOLIO, F. – MADSEN, H. A. – FISCHER, A. – BAK, CH. 2017. A semi-empirical airfoil stall noise model based on surface pressure measurements. In Journal of Sound and Vibration, vol. 387, pp. 127–162. DOI: https://doi.org/10.1016/j.jsv.2016.09.033

BUILO, S. I. 2013. Physical, mechanical and statistical aspects of acoustic emission diagnostics. In Physics and Mechanics of New Materials and Their Applications. New York : Nova Science Publishers, no. 15, pp. 171–184.

DANYUK, A. – MERSON, D. – VINOGRADOV, A. 2014. New prospects to use acoustic emission during scratch testing for probing fundamental mechanisms of plastic deformation. In The 12th International Conference of the Slovenian Society for Non-Destructive Testing "Application of Contemporary Non-Destructive Testing in Engineering", 4–6 September 2013, Portorož, Slovenia, pp. 567–574.

DANYUK, A. V. – RASTEGAEV, I. A. – MERSON, D. L. – VINOGRADOV, A. 2017. Advanced-reliability acoustic-emission transducers. In Russian Journal of Nondestructive Testing, vol. 53, no. 1, pp. 32–38.

CHAN, P. K. – STOLFO, S. J. 1998. Toward scalable learning with non-uniform class and cost distributions: A case study in credit card fraud detection. In KDD´98 Proceedings of the 4th International

Conference on Knowledge Discovery and Data Mining, New York, USA, 27–31 August 1998, pp. 164–168.

GLOWACZ, A. 2018. Acoustic based fault diagnosis of three-phase induction motor. In Applied Acoustics, vol. 137, pp. 82–89. DOI: https://doi.org/10.1016/j.apacoust.2018.03.010

JIANG, C. – SONG, Q. – GUO, D. – LI, H. 2014. Estimation algorithm of minimum dwell time in precision cylindrical plunge grinding using acoustic emission signal. In International Journal of Precision Engineering and Manufacturing, vol. 15, pp. 601–607. DOI: https://doi.org/10.1007/s12541-014-0377-y

KOVACEVIC, R. – MOMBER, A. W. – MOHEN, R. S. 2002. Energy dissipation control in hydro-abrasive machining using quantitative acoustic emission. In The International Journal of Advanced Manufacturing Technology, vol. 20, no. 6, pp. 397–406. DOI: https://doi.org/10.1007/s001700200169

LACAGNINA, G. – CHAITANYA, P. – KIM, J.-H. – BERK, T. – JOSEPH, P. – CHOI, K.-S. GANAPATHISUBRAMANI, B. – HASHEMINEJAD, S. M. – CHONG, T. P. – STALNOV, O. SHAHAB, M. F. – OMIDYEGANEH, M. – PINELLI. A. 2021. Leading edge serrations for the reduction of aerofoil self-noise at low angle of attack, pre-stall and post-stall conditions. In International Journal of Aeroacoustics, vol. 20, no. 1–2, pp. 130–156. DOI: https://doi.org/10.1177/1475472X20978379

LIU, J. – JIANG, C. – YANG, X. – SUN, S. 2024. Review of the application of acoustic emission technology in green manufacturing. In International Journal of Precision Engineering and Manufacturing-Green Technology, vol. 11, no. 3, pp. 995–1016. DOI: https://doi.org/10.1007/s40684-023-00557-w

NARAYANAN, S. – SINGH, S. K. – KANT, M. – NARAYANMURTHY, A. 2024. Control of fan broadband noise through wavy leading and trailing edge serrations. In International Journal of Aeroacoustics, vol. 24, no. 1–2, pp. 90–103. DOI: https://doi.org/10.1177/1475472X241306316

NASHED, M. S. – STEEL, J. A. – REUBEN, R. L. 2013. The use of acoustic emission for the condition assessment of gas turbines: Acoustic emission generation from normal running. In Proceedings of the Institution of Mechanical Engineers, Part E: Journal of Process Mechanical Engineering, vol. 228, no. 4, pp. 286–308. DOI: https://doi.org/10.1177/0954408913502167

O´BRIEN, R. J. – FONTANA, J. M. – PONSO, N. – MOLISANI, L. 2017. A pattern recognition system based on acoustic signals for fault detection on composite materials. In European Journal of Mechanics – A/Solids, vol. 64, pp. 1–10. DOI: https://doi.org/10.1016/j.euromechsol.2017.01.007

OHTSU, M. 2015. Acoustic Emission (AE) and Related Non-destructive Evaluation (NDE) Techniques in the Fracture Mechanics of Concrete. Fundamentals and Applications. UK : Elsevier, Woodhead Publishing, 318 pp. ISBN 978-1-78242-327-0. DOI: https://doi.org/10.1016/C2014-0-02667-6

POMPONI, E. – VINOGRADOV, A. – DANYUK, A. 2015. Wavelet based approach to signal activity detection and phase picking: Application to acoustic emission. In Signal Processing, no. 115, pp. 110–119. DOI: https://doi.org/10.1016/j.sigpro.2015.03.016

POMPONI, E. – VINOGRADOV, A. 2013. A real-time approach to acoustic emission clustering. In Mechanical Systems and Signal Processing, vol. 40, no. 2, pp. 791–804. DOI: https://doi.org/10.1016/j.ymssp.2013.03.017

RANI, M. – DHOK, S. – DESHMUKH, R. 2020. A machine condition monitoring framework using compressed signal processing. In Sensors, vol. 20, no. 1, article no. 319. DOI: https://doi.org/10.3390/s20010319

SHAO, H. – JIANG, H. – LI, X. – WU, S. 2018. Intelligent fault diagnosis of rolling bearing using deep wavelet auto-encoder with extreme learning machine. In Knowledge-Based Systems, vol. 140, pp. 1–14. DOI: https://doi.org/10.1016/j.knosys.2017.10.024

ZHANG, Y. – WANG, T. – PAN, W.-P. – ROMERO, C. E. 2019a. Advances in Ultra-Low Emission Control Technologies for Coal-Fired Power Plants. UK : Elsevier, Woodhead Publishing, 273 pp. ISBN 978-0-08-102418-8. DOI: https://doi.org/10.1016/C2017-0-00932-1

ZHANG, J. – YANG, S. – HAO, R. – GU, X. 2019b. Amplitude attenuation laws of acoustic emission waves in plate structures. In Dyna, vol. 94, no. 1, pp. 67–74. DOI: http://dx.doi.org/10.6036/8987

ZHAO, X. – JIA, M. – LIN, M. 2020. Deep Laplacian Auto-encoder and its application into imbalanced fault diagnosis of rotating machinery. In Measurement, vol. 152, article no. 107320. DOI: https://doi.org/10.1016/j.measurement.2019.107320

ŽITŇÁK, M. – LENDELOVÁ, J. – PIVARČIOVÁ, Z. – KORENKO, M. – KIEŁBASA, P. – DOSTÁL, P. 2023. Possibilties of noise load elemination in production. In Acta Technologica Agriculturae, vol. 26, no. 1, pp. 42–48. DOI: https://doi.org/10.2478/ata-2023-0006

WANG, W.-J. – CUI, L.-L. – CHEN, D.-Y. 2016. Multi-scale morphology analysis of acoustic emission signal and quantitative diagnosis for bearing fault. In Acta Mechanica Sinica, vol. 32, pp. 265–272. DOI: https://doi.org/10.1007/s10409-015-0529-z

WU, Z. – GUO, Y. – LIN, W. – YU, S. – JI, Y. 2018. A weighted deep representation learning model for imbalanced fault diagnosis in cyber-physical systems. In Sensors, vol. 18, no. 4, article no. 1096. DOI: https://doi.org/10.3390/s18041096

XU, B. – WU, J. – WANG, M. 2017. Study of modal acoustic emission to monitor the impact damage in a composite plate. In Journal of Vibroengineering, vol. 19, no. 5, pp. 3335–3348. DOI: https://doi.org/10.21595/jve.2017.17879